Physics and Chemistry of Minerals (2020) 47:23
https://doi.org/10.1007/s00269-020-01092-9

ORIGINAL PAPER

Raman spectra of sillimanite, andalusite, and kyanite at various temperatures

Kuan Zhai[1,2] · Weihong Xue[1] · Hu Wang[3] · Xiang Wu[3] · Shuangmeng Zhai[1]

Received: 5 January 2020 / Accepted: 19 April 2020

Abstract
High-temperature Raman spectra of natural sillimanite, andalusite and kyanite were measured in the temperature range of 296–1273 K at ambient pressure. No phase transition was observed over the temperature range in this study. Raman modes for the three samples vary with temperature linearly. The temperature and pressure dependence of the force constants for Si–O stretching vibrations in Al_2SiO_5 polymorphs were determined. The isobaric mode Grüneisen parameters of sillimanite, andalusite, and kyanite were determined from the temperature dependent of present high-temperature Raman spectra and previous results of thermal expansion coefficients. The intrinsic anharmonic mode parameters were estimated and nonzero, indicating the existence of intrinsic anharmonicity for sillimanite, andalusite and kyanite. Based on Kieffer model, the thermodynamic parameters, including isochoric heat capacity and entropy, were calculated.

Keywords Sillimanite · Andalusite · Kyanite · Al_2SiO_5 · Raman spectra · Various temperatures

Introduction

Sillimanite, andalusite, and kyanite, the three Al_2SiO_5 polymorphs are known as important minerals in metamorphosed aluminous rocks, such as metapelitic schist and micaceous quartzite. These polymorphs are of great importance due to their use as primary thermobarometers of metamorphic rocks based on their thermodynamic properties (Kerrick 1990), as they provide information about pressure–temperature (*P*–*T*) conditions (Wu and Zhao 2007). The crystal structures of sillimanite, andalusite, and kyanite are well determined (Burnham and Buerger 1961; Burnham 1963a, b), as shown in Fig. 1. In each structure of Al_2SiO_5 polymorphs, all the Si^{4+} cations surround by four O^{2-} anions, half of the Al^{3+} cations are in octahedral coordination that composed the aluminum oxide octahedra chain along *c*-axis, and the remaining Al^{3+} is four-, five-, six-coordinated in sillimanite, andalusite and kyanite, respectively (Winter and Ghose 1979).

The stabilities and physical properties of sillimanite, andalusite, and kyanite have been widely investigated in previous studies. At ambient pressure, kyanite begins to decompose at ~ 1423 K and completes at ~ 1623 K, andalusite starts to decompose to a mixture of mullite plus silica at ~ 1523 K and fully decomposes at ~ 1723 K, and sillimanite is the least likely to decompose and its fully decomposed temperature is about 1923 K (Schneider and Majdic 1979, 1980, 1981; Aguilar-Santillan et al. 2002; Bradt 2008). The phase diagram of sillimanite, andalusite and kyanite has been well constrained (Bell 1963; Richardson et al. 1969; Holdaway 1971; Bohlen et al. 1991). Under high-pressure and high-temperature conditions, kyanite decomposes into stishovite and corundum (Liu 1974; Schmidt et al. 1997; Liu et al. 2006; Ono et al. 2007). Recently kyanite was found to transform into two new high-pressure and high-temperature phases, kyanite II and kyanite III, ranging from 13–24 GPa and above 2300–2500 K (Zhou et al. 2018). The physical properties including compressibility, heat capacity, entropy and thermal expansivity of sillimanite, andalusite and kyanite were reported in many literatures (Skinner et al.

✉ Weihong Xue
xueweihong@mail.gyig.ac.cn

[1] Key Laboratory of High-Temperature and High-Pressure Study of the Earth's Interior, Institute of Geochemistry, Chinese Academy of Sciences, Guiyang 550081, Guizhou, China

[2] University of Chinese Academy of Sciences, Beijing 100049, China

[3] State Key Laboratory of Geological Processes and Mineral Resources, China University of Geosciences, Wuhan 430074, China

Published online: 02 May 2020

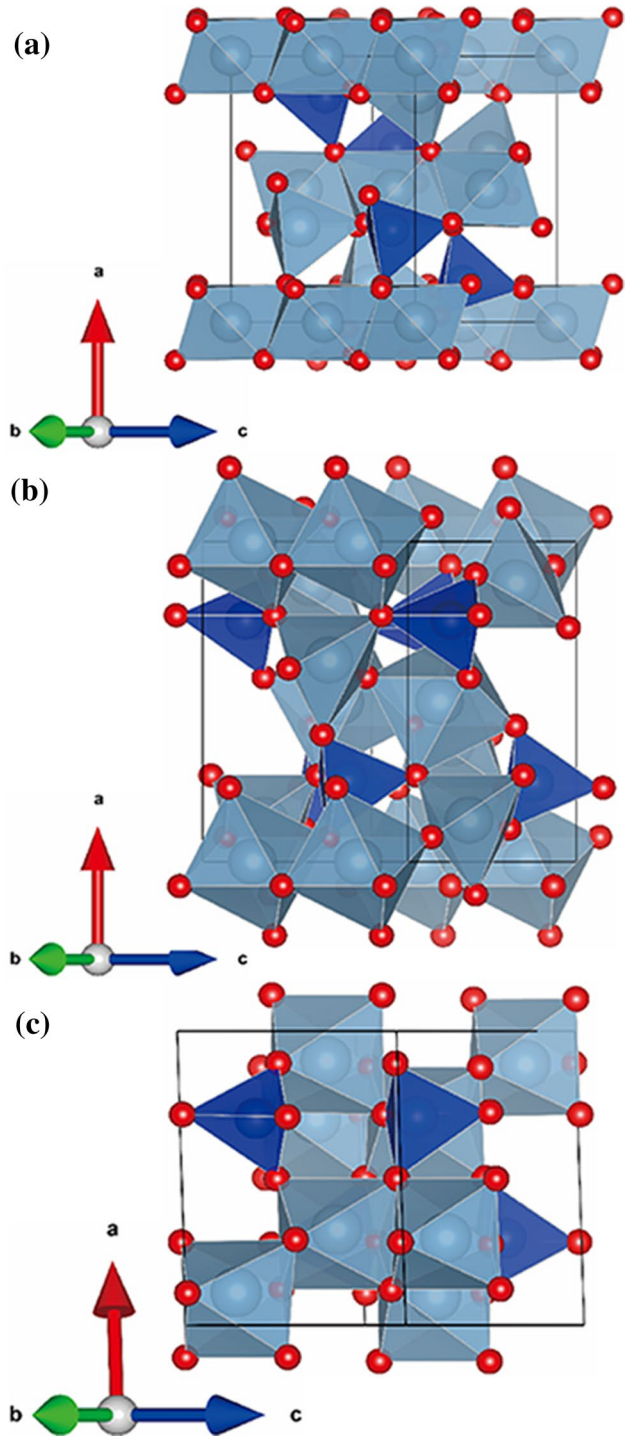

Fig. 1 The crystal structures of sillimanite (**a**), andalusite (**b**) and kyanite (**c**). The images were obtained using VESTA program (Momma and Izumi 2011)

1961; Pankratz and Kelley 1964; Brace et al. 1969; Vaughan and Weidner 1978; Ralph et al. 1984; Robie and Hemingway 1984; Salje 1986; Hemingway et al. 1991; Irifune et al. 1995; Matsui 1996; Comodi et al. 1997; Yang et al. 1997a, b; Oganov and Brodholt 2000; Winkler et al. 2001; Friedrich et al. 2004; Burt et al. 2006; Gatta et al. 2006; Liu et al. 2009, 2010; Hu et al. 2011; Fortes 2019).

Raman spectroscopy has become a common spectroscopic technique to understand the thermodynamic properties of minerals. Compared with X-ray diffraction, Raman spectra reveal the detailed information on the interactions of ensembles of atoms, and provide constraints on thermodynamic properties at high-temperature and high pressure conditions. High pressure Raman spectra of Al_2SiO_5 polymorphs have already been collected and analyzed up to about 10.5 GPa (Mernagh and Liu 1991). However, the effect of temperature on the Raman spectra of Al_2SiO_5 polymorphs is not well understood though the high-temperature Raman spectra of andalusite were measured up to 873 K (Iishi et al. 1979). In this study, the Micro-Raman spectra of three Al_2SiO_5 polymorphs at various temperatures up to 1273 K were recorded at ambient pressure, and the effects of temperature on vibrational modes as well as the isobaric mode Grüneisen parameters of sillimanite, andalusite, and kyanite were calculated. Based on the present study and previous results, the evolution of the force constant with temperature and pressure was estimated, and the intrinsic anharmonicity was determined which are predominant for constraining the thermodynamic property.

Experimental

The natural sillimanite, andalusite, and kyanite samples from Sri Lanka, USA, and Switzerland, respectively, were used for high-temperature Raman spectroscopic measurements. The chemical formula of the natural sillimanite, andalusite, and kyanite were $Al_{2.01}Si_{0.99}O_5$, Al_2SiO_5, and $Al_{2.02}Si_{0.98}O_5$, respectively, as reported by RRUFF Project. The more details of the three samples are shown in the RRUFF database as R060787, R050258, and R050450, respectively (https://rruff.info).

The high-temperature Raman spectra at ambient pressure were collected from 100 to 1200 cm^{-1} via a Horiba Jobin Yvon Raman spectroscope equipped with an 1800 g/mm double-grating. Samples were excited by a frequency-doubled Nd:YAG laser ($\lambda = 532$ nm) operated at 20 mW through an SLM Plan 50 × Olympus microscope objective. The spectrometer was calibrated with a silicon wafer focused and collected as a static spectrum centered at 521 cm^{-1}. High-temperature (HT) Raman spectra were obtained using a Linkam TS 1500 heating stage and a Raman spectroscope. The method and heating procedure were similar to a previous study (Xue et al. 2018). Three small different Al_2SiO_5 fragments of the three phases were heated by a resistance heater which was controlled by an automatic temperature controlling unit and the temperature accuracy is better than

1 K. The high-temperature spectroscopic measurement system has been calibrated and the errors due to horizontal thermal gradients were smaller than 1%. For thermal equilibrium, the spectra were collected after maintaining at each temperature for 10–15 min. The accumulation time for each spectrum was 120 s. The analyses of Raman spectra by Lorentzian curve fitting were performed using the PeakFit program (Systat Software, San Jose, CA, USA).

Results and discussion

It is known that an isolated SiO_4 tetrahedra has T_d symmetry and four vibrational normal modes: $v_3(T_2) = 956\ cm^{-1}$, $v_1(A_1) = 819\ cm^{-1}$, $v_4(T_2) = 527\ cm^{-1}$ and $v_2(E) = 340\ cm^{-1}$ (Nakamoto 2009), where E and T_2 modes are doubly and triply degenerate, respectively. However, in Al_2SiO_5 polymorphs the T_d symmetry of a free tetrahedra $(SiO_4)^{4-}$ changed.

Sillimanite has an orthorhombic unit cell with space group of *Pnma* (Taylor 1928; Winter and Ghose 1979 and references therein). According to factor group theory, the Raman active vibrations of sillimanite are as follows (Salje and Werneke 1982):

$$\Gamma = 13A_g + 8B_{1g} + 13B_{2g} + 8B_{3g}.$$

Among these modes, 42 modes that belong to the irreducible representation A_g, B_{1g}, B_{2g}, B_{3g} are Raman active.

Andalusite has an orthorhombic structure with *Pnnm* space group (Taylor 1929; Burnham and Buerger 1961; Winter and Ghose 1979). The Raman mode obtained from a factor group analysis is (Iishi et al. 1979):

$$\Gamma = 14A_g + 14B_{1g} + 10B_{2g} + 10B_{3g}.$$

Hence, 48 Raman active modes are predicted.

Kyanite crystallizes in the space group $P\bar{1}$ (Náray-Szabo et al. 1929; Winter and Ghose 1979). From the group theoretical analysis, 48 theoretical vibrational modes at room temperature as reported earlier are (Rao et al. 1999):

$$\Gamma = 48A_g.$$

The Raman spectra of sillimanite, andalusite, and kyanite at ambient conditions are plotted in Fig. 2. Although up to 48 Raman active vibrational modes are predicted, only 11–15 Raman active modes were reliably distinguished due to the very low intensity of some vibrations and/or their partial overlap.

For Al_2SiO_5, the spectra show marked change as the coordination number of the aluminum changes. Si–O bonds have stronger force constants than Al-O bonds, so that the Si–O tetrahedra vibrate at higher energies. In addition, the presence of Al^{IV} causes the stretching vibration of non-bridging

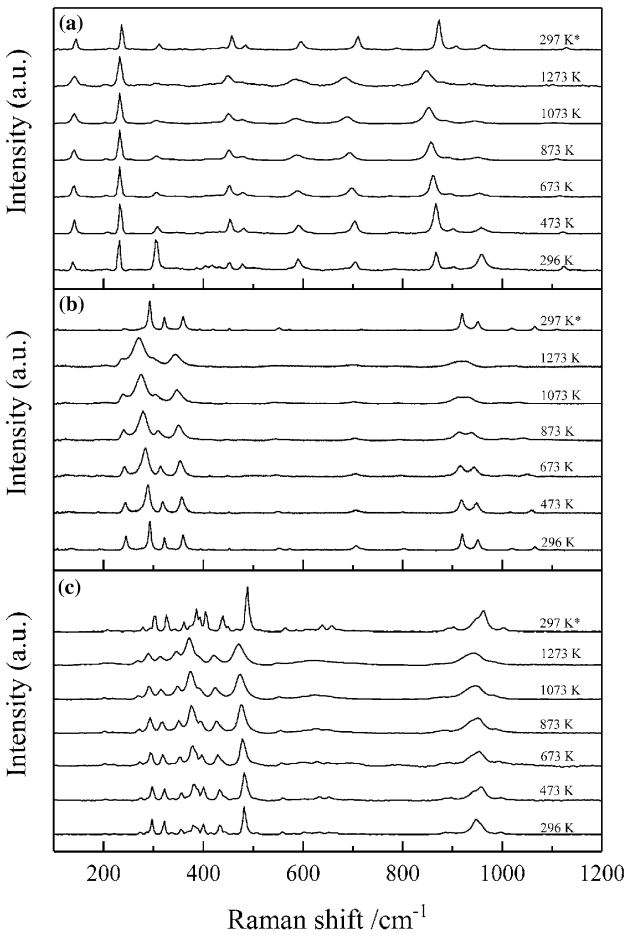

Fig. 2 Typical Raman spectra of sillimanite (**a**), andalusite (**b**) and kyanite (**c**) at various temperatures and ambient pressure. The temperature values with asterisk symbol represent the Raman spectra collected after cooling to room temperature

oxygen in the isolated SiO_4 tetrahedral to move to the higher frequency range.

Sillimanite is a typical orthosilicate, and the stretching modes of the SiO_4 tetrahedra occur between 800 and 1200 cm^{-1} (Iishi et al. 1979; Salje and Werneke 1982). Mernagh and Liu (1991) proposed the Raman modes at 485 cm^{-1} for v_2 mode of free SiO_4 ion. The Al-O vibrational modes appear in the same region as internal bending modes of SiO_4 tetrahedra (Iishi et al 1979), and the band at 789, 710 and 596 cm^{-1} are assigned to Al-O bending mode (Lazarev 1972). While those below 400 cm^{-1} (312, 237 and 144 cm^{-1}) are associated with the lattice vibrations. Andalusite also shows characteristics of an orthosilicate, the stretching modes of SiO_4 also observed above 800 cm^{-1}, the bending mode of SiO_4 around 360 cm^{-1}. And the bands in the 500–700 cm^{-1} attributes to Al-O vibrations (Lazarev 1972; Iishi et al. 1979; Pan et al. 2006). As above, four bands in the range 9000–1040 cm^{-1} corresponding to the stretching modes of Si–O bands in kyanite (McMillan et al. 1982). The

Al-O bands occur at lower frequencies in kyanite than sillimanite and andalusite, such as a Raman band at 488 cm^{-1} for bending mode of Al^{VI}–O–Si. Owing to the poor symmetry and poor degeneracy, there are several other Raman bands in the range from 200 to 400 cm^{-1} attribute to bending mode of Al^{VI}–O.

Temperature dependence of Raman spectra

The typical Raman spectra of sillimanite, andalusite, and kyanite at various temperatures and ambient pressure are illustrated in Fig. 2. Obviously, all the Raman bands of Al_2SiO_5 polymorphs show red shift, most modes become weak and broaden but several peaks are too weak to be detected upon increasing temperatures. Neither new band nor splitting was observed. The continuous changes imply successive variation of Al_2SiO_5 polymorphs but without evident phase transition, which is in general agreement with previous studies about phase transition (Schneider and Majdic 1979, 1980, 1981; Aguilar-Santillan et al. 2002).

The variations of Raman modes at different temperatures for all measurable modes are illustrated in Fig. 3. With a linear regression of $v_i = a_i + b_i T$ for each mode, all vibrational modes systematically show negative temperature dependences. The temperature coefficients (b_i) of the Raman vibrations are listed in Table 1. The temperature-induced frequency shifts due to increasing bond length of Si–O and Al–O bonds. The fitting parameters values (b_i) for sillimanite, andalusite and kyanite vary from $-3.05(5)$ to $-0.32(1)\times10^{-2}$ cm^{-1} K^{-1}, $-4.29(3)$ to $-0.70(1)\times10^{-2}$ cm^{-1} K^{-1} and $-3.22(1)$ to $-1.02(6)\times10^{-2}$ cm^{-1} K^{-1}, respectively. Also, the values of b_i indicate the internal modes of SiO_4 and Al–O polyhedra are sensitive to temperature compared with rotational or translational lattice modes.

Temperature and pressure dependence of the force constant *k*

The force constant, k, representing the interaction between nearest atoms and determined by bond length and bond angle, is used to analyze the lattice dynamics. For the simplest case of a vibrating diatomic species, the bond force constant, k (typically in N/m), is related to the vibrational modes and could be expressed approximately using the formula according to Hooke's Law (Okada et al. 2008):

$$k = 4\pi^2 c^2 \mu v^2,$$

where v is the vibrational frequency of the stretching band, c is the velocity of light in vacuum (2.998×10^8 m/s), and μ is the reduced mass of the vibrating atoms.

We calculated k from the stretching modes at various temperatures and pressures, as shown in Figs. 4 and 5. Since v_3 asymmetric stretching vibrations located in higher frequency range than that of v_1 symmetric stretching mode, the force constants of v_3 vibrations are larger than that of v_1 mode. The high-pressure Raman data reported by Mernagh

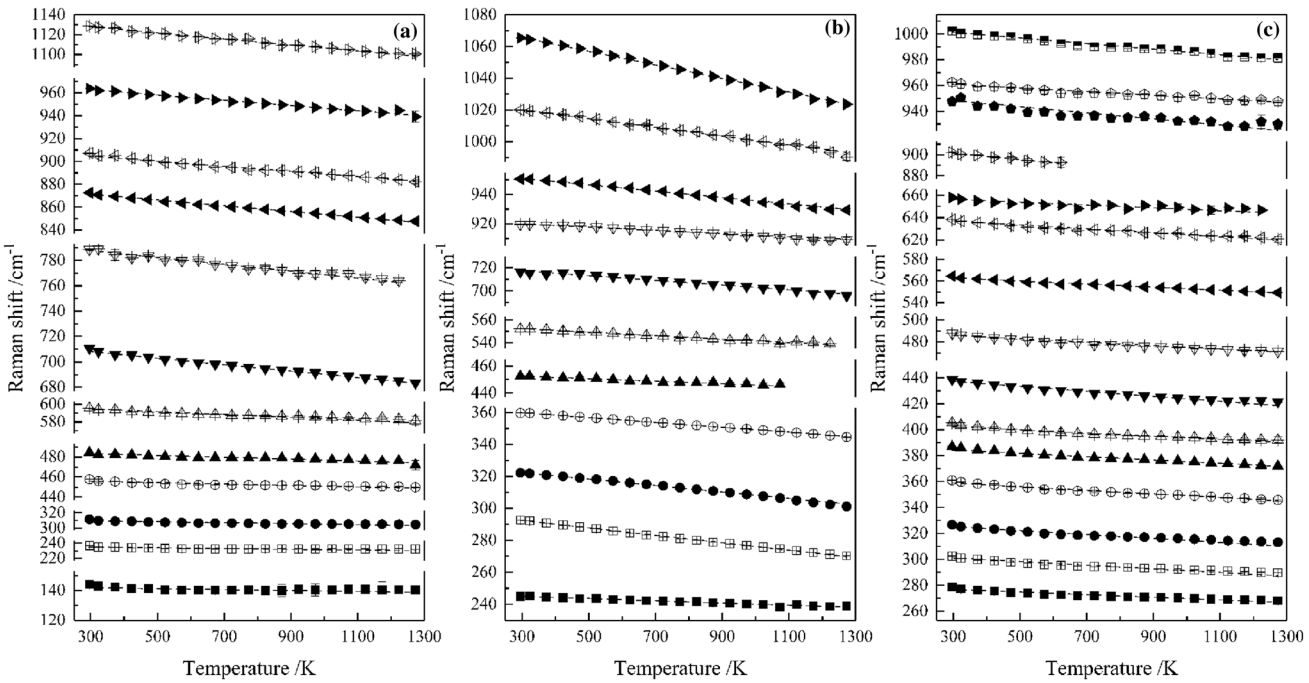

Fig. 3 Temperature dependence of the Raman modes of sillimanite (**a**), andalusite (**b**) and kyanite (**c**) at ambient pressure

Table 1 Constants determined in $v_i = a_i + b_i T$ at ambient pressure and the values of γ_{iT}, γ_{iP} and β_i of Al_2SiO_5

Sillimanite							Andalusite							Kyanite						
v_i	a_i	$-b_i \times 10^2$	R^2	γ_{iP}	γ_{iT}^*	$\beta_i \times 10^5$	v_i	a_i	$-b_i \times 10^2$	R^2	γ_{iP}	γ_{iT}^*	$\beta_i \times 10^5$	v_i	a_i	$-b_i \times 10^2$	R^2	γ_{iP}	γ_{iT}^*	$\beta_i \times 10^5$
1129	1137.1(4)	3.05(5)	0.993	1.56	0.61	− 1.65	1065	1078.4(1)	4.29(3)	0.999	1.55			1002	1008.2(3)	2.23(6)	0.987	0.86		
964	969.7(4)	2.31(5)	0.990	1.39	0.95	− 0.75	1020	1028.3(1)	2.77(3)	0.998	1.04			963	967.0(3)	1.65(6)	0.979	0.66		
907	911.3(5)	2.22(5)	0.986	1.41			950	957.5(2)	2.17(4)	0.994	0.88			948	956.0(9)	2.42(1)	0.908	0.99	0.73	− 0.66
872	879.2(3)	2.54(4)	0.992	1.68	0.94	− 1.29	919	924.3(2)	1.44(4)	0.981	0.60	0.66	0.15	902	911.4(7)	3.22(1)	0.976	1.38		
789	796.0(6)	2.72(1)	0.972	1.99			716	723.5(5)	2.04(7)	0.974	1.10			658	665.7(12)	2.78(3)	0.939	1.64	0.59	− 2.71
710	715.7(4)	2.54(6)	0.987	2.07	0.74	− 2.30	552	556.6(1)	1.41(2)	0.996	0.98			638	642.5(4)	1.80(7)	0.971	1.09		
596	599.8(5)	1.61(1)	0.920	1.56	0.69	− 1.51	452	456.6(1)	1.23(2)	0.994	1.05	0.89	− 0.40	565	567.3(2)	1.43(3)	0.989	0.98	0.72	− 0.68
485	486.4(5)	0.94(8)	0.873	1.12	1.89	1.34	359	364.4(1)	1.52(1)	0.999	1.63	0.68	− 2.45	488	491.2(5)	1.63(6)	0.988	1.30	0.91	− 0.99
458	458.0(6)	0.72(8)	0.772	0.91	0.29	− 1.08	322	329.5(1)	2.32(2)	0.999	2.77	0.67	− 5.45	439	443.1(5)	1.93(9)	0.951	1.70	1.19	− 1.33
312	311.5(2)	0.63(4)	0.914	1.17	− 0.47	− 2.84	293	299.5(1)	2.33(1)	0.999	3.06	1.03	− 5.27	405	406.6(6)	1.28(8)	0.925	1.22	1.05	− 0.46
237	236.3(7)	0.49(1)	0.532	1.20	− 0.90	− 3.63	245	247.1(1)	0.70(1)	0.985	1.10			387	388.1(3)	1.27(3)	0.984	1.27	0.60	− 1.74
144	142.8(7)	0.32(1)	0.273	1.29	0.02	− 2.18								361	362.6(3)	1.37(5)	0.980	1.47	0.86	− 1.59
														327	329.9(4)	1.53(9)	0.932	1.81	1.24	− 1.48
														302	305.5(5)	1.43(8)	0.937	1.83	1.21	− 1.60
														279	280.0(4)	1.02(6)	0.935	1.42		
Average				1.45	0.48	− 1.59					1.43	0.79	− 2.69					1.31	1.01	− 1.47

v_i and a_i are in cm^{-1}, T in K, $b_i = (\partial v_i / \partial T)_P$, b_i in $cm^{-1}\ K^{-1}$. R^2 is the correlation coefficient. γ_{iT}^* are recalculate from Mernagh and Liu (1991)

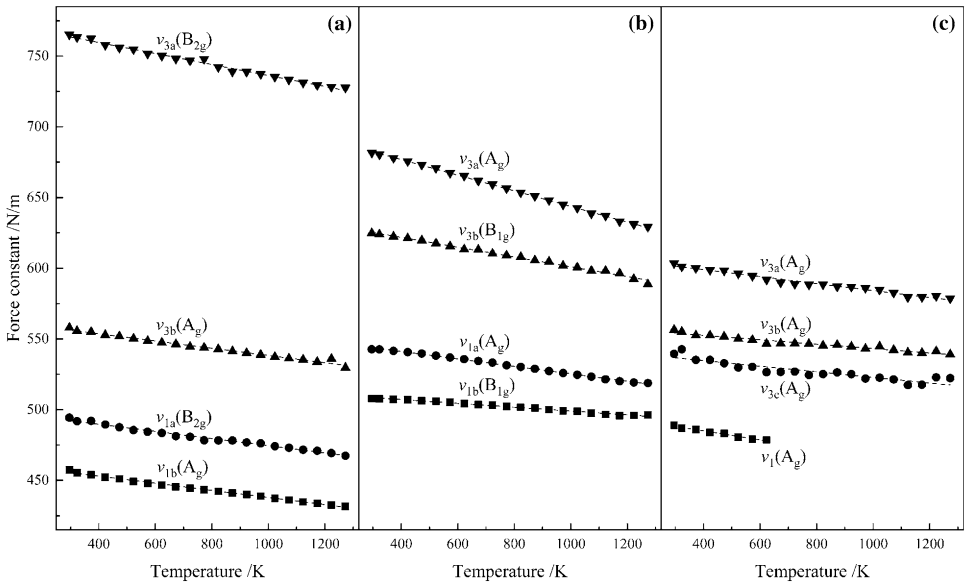

Fig. 4 Evolution of the force constant of different stretching modes in sillimanite (**a**), andalusite (**b**) and kyanite (**c**), *k*, with temperature

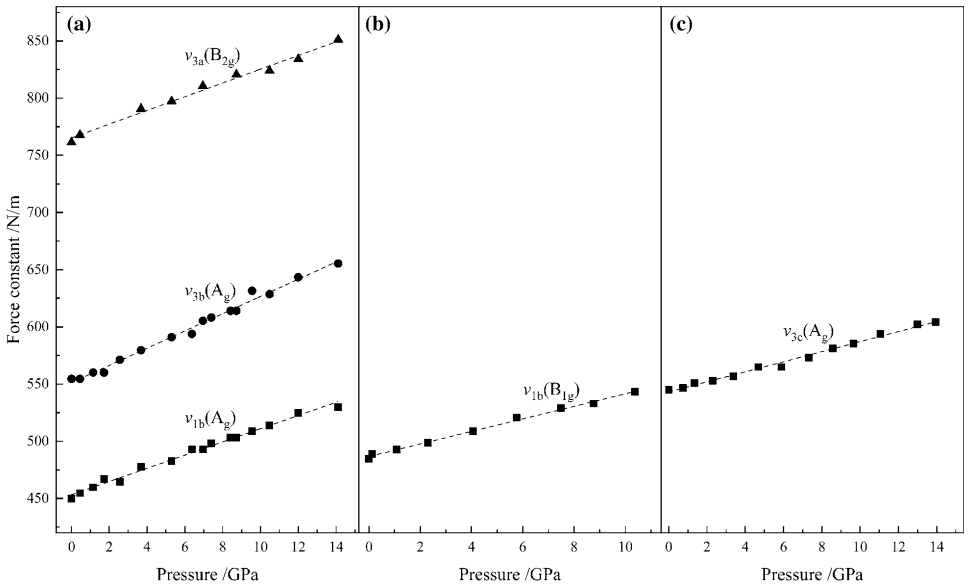

Fig. 5 Evolution of the force constant of different stretching modes in sillimanite (**a**), andalusite (**b**) and kyanite (**c**), *k*, with pressure. The original high-pressure data was from Mernagh and Liu (1991)

and Liu (1991) were adopted for pressure evolution of bond force constant. However, fewer bands were observed in high-pressure Raman spectra due to the presence of a high fluorescent background in the Raman spectra recorded from the diamond-anvil cell in the study of Mernagh and Liu (1991).

The temperature and pressure derivatives of *k* are listed in Table 2. Generally, the large variation of *k* with temperature can be attributed to weakness of the bond strength (Okada et al. 2008). The higher absolute $\delta k/\delta T$ indicating the rate of the bond length becomes long is high. On contrast, the higher absolute $\delta k/\delta P$ indicating that the rate at which the bond length becomes short is higher. For Si–O bonds in SiO_4 tetrahedron of Al_2SiO_5, the absolute $\delta k/\delta T$ of v_3 is higher than that of v_1 in sillimanite and andalusite, whereas the absolute $\delta k/\delta T$ of v_3 is smaller than that of v_1 in kyanite. Based on a comparison between the results shown in Fig. 5, the trend of the pressure derivatives of *k*, $\delta k/\delta P$, is the same as that of the above-mentioned $\delta k/\delta T$. Owing to fewer bands for andalusite and kyanite, it is impossible to compare the pressure derivatives of *k* for the different stretching modes in andalusite and kyanite. For Si–O bonds in SiO_4 tetrahedron of sillimanite, the $\delta k/\delta P$ of v_3 asymmetric stretching mode is higher than v_1 symmetric stretching mode.

Isobaric Grüneisen parameters

The Grüneisen parameter, γ, is an important physics quantum to describe the elasticity and anharmonicity of the thermodynamic properties under high temperature and high pressure of the solid. The temperature derivatives of

Table 2 Temperature and pressure derivatives of force constant k based on Si–O stretching modes in Al_2SiO_5

Sillimanite			Andalusite			Kyanite		
Vibrations (cm^{-1})	$-(\delta k/\delta T)$ (10^{-2} N m^{-1} K^{-1})	$(\delta k/\delta P)$[a] (N m^{-1} GPa^{-1})	Vibrations (cm^{-1})	$-(\delta k/\delta T)$ (10^{-2} N m^{-1} K^{-1})	$(\delta k/\delta P)$[a] (N m^{-1} GPa^{-1})	Vibrations (cm^{-1})	$-(\delta k/\delta T)$ (10^{-2} N m^{-1} K^{-1})	$(\delta k/\delta P)$[a] (N m^{-1} GPa^{-1})
1129	3.89(8)	6.00(2)	1065	5.52(3)		1002	2.46(9)	
964	2.56(7)	7.53(1)	1020	3.47(3)		963	1.56(8)	
907	2.53(7)		950	2.63(2)		948	1.98(2)	4.39(1)
872	2.52(3)	5.77(1)	919	1.36 (3)	5.48(1)	902	3.19(1)	

[a]Calculated using the high-pressure Raman data from Mernagh and Liu (1991)

different Raman modes can be adopted to calculate the isobaric mode Grüneisen parameter, γ_{iP}, defined as the following expression (Gillet et al. 1989; Okada et al. 2008):

$$\gamma_{iP} = -\frac{1}{\alpha v_i}\left(\frac{\partial vi}{\partial T}\right)_P,$$

where v_i is the vibrational frequency of the ith band and α is the volume thermal expansion coefficient. The volume thermal expansion coefficient α of a material is defined as $\alpha = \frac{1}{V}\left(\frac{\partial V}{\partial T}\right)_P$, and is measured experimentally by the evolution of the sample volume with temperature. If the volume thermal expansion coefficient α does not change with temperature, then integration gives (Fei 1995):

$$\ln \frac{V}{V_0} = \alpha(T - T_0).$$

The thermal expansion coefficient α of sillimanite, andalusite and kyanite were recalculated based on refine lattice parameters reported by Fortes (2019) as $1.73(2)\times10^{-5}$ K^{-1}, $2.60(2)\times10^{-5}$ K^{-1} and $2.58(2)\times10^{-5}$ K^{-1}, respectively.

The recalculated values of γ_{iP} for different vibrational modes of sillimanite, andalusite and kyanite are also listed in Table 1, ranging from 0.91 to 2.07, 0.60 to 3.06, and 0.66 to 1.83, respectively. Moreover, the average values of γ_{iP} for sillimanite, andalusite and kyanite are 1.45, 1.43 and 1.31, respectively. The internal vibrations of sillimanite show larger isobaric mode Grüneisen parameters than those of external vibrations. However, andalusite and kyanite show opposite result to sillimanite, but consistent with those of forsterite (Reynard et al. 1992).

Anharmonicity

Different values between isothermal mode Grüneisen parameters and isobaric mode Grüneisen parameters suggest an intrinsic anharmonicity exists, which expresses a change in frequency induced by temperature at constant volume.

The intrinsic anharmonic mode parameter, β_i, which is defined by Mammone and Sharma (1979), correlating with thermal expansion, the isothermal and isobaric mode Grüneisen parameters can be expressed as:

$$\beta_i = \alpha(\gamma_{iT} - \gamma_{iP}).$$

The isothermal mode Grüneisen, γ_{iT}, describing the pressure dependences of the vibrational mode, is defined as (Gillet et al. 1989):

$$\gamma_{iT} = -\frac{K_T}{v_i}\left(\frac{\partial vi}{\partial P}\right)_T,$$

where K_T is the isothermal bulk modulus. The pressure derived values $(\partial v_i/\partial P)_T$ for Al_2SiO_5 polymorphs have been reported (Mernagh and Liu 1991). Using the latest reported isothermal bulk moduli K_T (Burt et al. 2006; Liu et al. 2009), we further recalculate the isothermal mode Grüneisen (γ_{iT}), which are also reported in Table 1. The values of calculated intrinsic anharmonic mode parameters β_i of each vibrational band are nonzero and reported in Table 1 as well. Generally, almost all the absolute values of β_i in three Al_2SiO_5 polymorph is higher for low-frequency modes than for the high-frequency modes, as observed in end-member garnet (Gillet et al. 1992), reflecting the important instability of the low-frequency mode. The internal mode of the SiO_4 tetrahedra will be more stable due to the stronger bond to reduce the effect of temperature on vibrational mode.

Heat capacity

The Kieffer's lattice vibrational model use a rather simplified density of state for phonon dispersion to give an accurate approximation of heat capacity. The phonon density of state consist acoustic modes derived from the elastic constants and the optic modes from the Raman and IR spectra (Kieffer 1979a, b).

As each Al_2SiO_5 polymorphs unit cell contains four formula unit, 96 lattice vibrational modes are permitted. Among them three acoustic branches were characterized by the directionally averaged sound velocity u_1, u_2 (shear branches), and u_3 (longitudinal branch) derived from elastic wave speeds which were calculated from the Birch (1961)

empirical relationship (Kojitani et al. 2003) and the equations A5 and A6 in Kieffer (1979a). The remaining modes were modeled as an optic continuum. The continuum was divided into several independent subinterval continua according to a similar mode assignment as the single continuum to achieve greater accuracy (Hofmeister and Chopelas 1991). Kieffer (1980) constructed a model with only one optic continuum to calculate the isochoric heat capacity C_v of the Al_2SiO_5 polymorphs based on Raman and IR spectra. Raman-active, IR-active and optic-inactive inferred from first-principle simulation can led a more proper Kieffer's model. In this study, the optic modes reported by Lv (2016) were adopted.

With the anharmonic contribution, the anharmonic isochoric heat capacity is

$$C_{V-\mathrm{An}} = 3nR\sum_{i=1}^{m} C_{Vi}(1-2\alpha_i T),$$

and C_{Vi} values can be estimated from the Einstein function:$C_{Vi} = k_{\mathrm{B}}\left(\frac{h\nu_i}{k_{\mathrm{B}}T}\right)^2 \mathrm{e}^{\left(\frac{h\nu_i}{k_{\mathrm{B}}T}\right)} / \left[\mathrm{e}^{\left(\frac{h\nu_i}{k_{\mathrm{B}}T}\right)} - 1\right]^2$,

where v_i is the vibrational frequency of ith mode given in 1/s, T is the temperature in K, while k_{B} and h are the Boltzmann and Plank constants, respectively. Thus, the anharmonic isochoric heat capacity could be obtained using the above method. The isochoric heat capacity and the anharmonic isochoric heat capacity were shown as the dotted line and solid line for Al_2SiO_5 polymorphs in Fig. 6, along with the C_v data calculated from the DSC measurement (Robie and Hemingway 1984; Hemingway et al. 1991).

In the harmonic approximation, isochoric heat capacity C_V tend to approach the classical Dulong-Petit limits (3nR) of Al_2SiO_5 polymorphs as 199.54 J/mol/K at high temperature. The anharmonic contribution becomes obvious with increasing temperature, the anharmonic isochoric heat capacity $C_{V\text{-An}}$ even exceed the Dulong-Petit limits above 1200 K, 1350 K, and 1300 K for sillimanite, andalusite, and kyanite, respectively. In addition, comparing the isochoric heat capacity C_v with the anharmonic isochoric heat capacity $C_{V\text{-An}}$, our results show good consistency with the calorimetric results (Robie and Hemingway 1984; Hemingway et al. 1991). Thus, the harmonic or quasi-harmonic approximation is not suitable at high temperatures, and the anharmonic effect can well explain the discrepancy between the calorimetric heat capacity and Dulong-Petit limits.

The isobaric heat capacity C_P is related to the isochoric heat capacity C_V by adding an anharmonic effect using the following equation:

$$C_P = C_V + \alpha T^2 K_{0,T} V_T T,$$

where α_T, $K_{0,T}$ and V_T were the thermal expansivity, isothermal bulk modulus, and volume at ambient pressure and T K, respectively. The temperature derivate of $K_{0,T}$ was supposed to the value of $K_{0,298}$. V_T was calculated with the following equation:

$$V_T = V_{298}\int_{298}^{T} \alpha_T \mathrm{d}T,$$

where V_{298} refers to the volume of the Al_2SiO_5 polymorphs at ambient conditions. The calculated C_P values are graphical illustrated in Fig. 7, along with the results from Robie and Hemingway (1984) and Hemingway et al. (1991). At low temperature, the C_P of Al_2SiO_5 polymorphs by the Kieffer model shows excellent agreement with the calorimetric data measured by Robie and Hemingway (1984), but differ from Hemingway et al. (1991) with increasing temperature. Actually, comparing the present C_P data with the DSC heat capacities (Hemingway et al. 1991), at the temperature of 1000 K, errors for sillimanite, andalusite, and kyanite were estimated to be ~ 4.07%, ~ 2.29%, and ~ 2.14%, respectively. Overall, our calculated C_P data fit well with calorimetry C_P values at relative low temperature which was identified as a reliable tool to predict the isobaric heat capacity C_P at comparative high temperature.

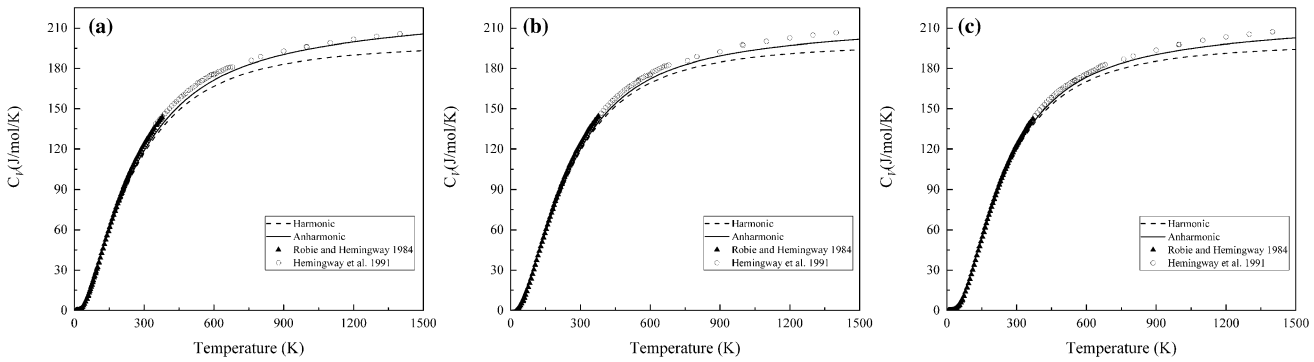

Fig. 6 Calculated harmonic and anharmonic isochoric heat capacity C_v of sillimanite (**a**), andalusite (**b**) and kyanite (**c**)

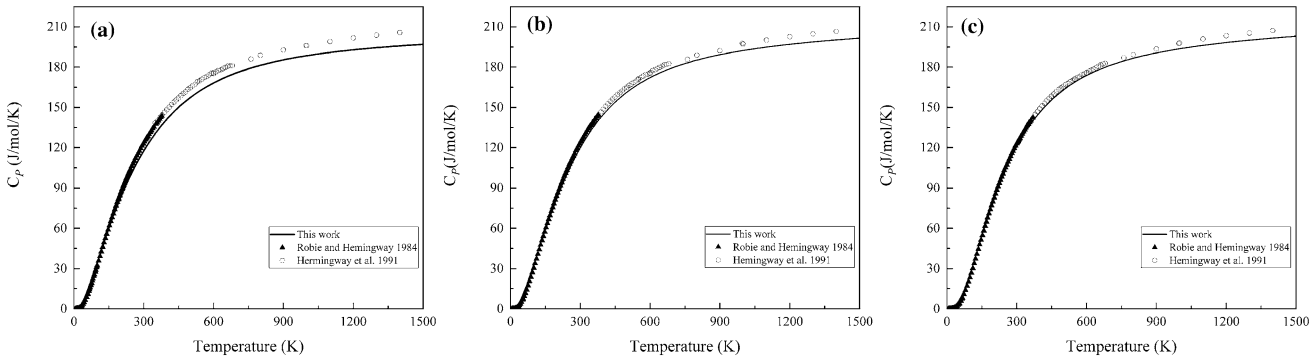

Fig. 7 Isobaric heat capacity C_P of of sillimanite (**a**), andalusite (**b**) and kyanite (**c**)

Table 3 The entropy (in J/mol/K) of sillimanite, andalusite and kyanite

Sillimanite	Andalusite	Kyanite	References
96.78	95.43	86.64	This study
96.15(1)	93.26(1)	83.80(8)	Todd (1950)
94.4	92.48	83.2	Kieffer (1980)
95.79(1)	91.39(1)	82.30(1)	Robie and Hemingway (1984)
97.68	91.39		Salje (1986)
95.40(5)	91.39(5)	82.80(5)	Hemingway et al. (1991)

Entropy

The obtained C_P values with the procedure mentioned above have been further used to determine vibrational entropy at T K using the following equation:

$$S_T^o = \int_0^T \frac{C_P}{T} dT.$$

In this work, the vibrational entropies at 298 K were compared with previous results in Table 3. Our calculated value of sillimanite shows good agreement with previous study (Todd 1950; Kieffer 1980; Robie and Hemingway 1984; Salje 1986; Hemingway et al. 1991). Salje (1986) once reported a biggest value as 101.12 J/mol/K, the discrepancy may due to the different chemical composition. In addition, the calculated values for andalusite and kyanite are slightly larger than the estimated values derived from low temperature heat capacity measurement (Todd 1950; Robie and Hemingway 1984; Kieffer 1980; Hemingway et al. 1991), suggesting that some of the thermodynamic data may influence the result, and the new values of entropy may be used as additional constraints on the slopes of the reaction boundaries estimated from phase equilibrium data.

Conclusion

In this study, the temperature-dependent Raman spectra of Al_2SiO_5 polymorphs (sillimanite, andalusite and kyanite) have been investigated from room temperature up to 1273 K at ambient pressure. All the lattice vibrational modes shift to lower frequency, the temperature coefficients reflect the sensitivity of the vibrational modes to temperature: internal modes > external modes. The force constant is an important factor determine the vibrational frequency, the force constant derived from Hooke's law can use to explain the lattice dynamic. The isobaric mode Grüneisen parameters are derived from the temperature dependence of the Raman active mode along, and the intrinsic anharmonic mode parameters are determined, which reflect the effect of the temperature on vibrational mode: the internal modes are more stable than external modes. The isochoric heat capacity and entropy of Al_2SiO_5 polymorphs are estimated by means of Kieffer model, and the anharmonic contribution was evaluated.

Acknowledgements This work was financially supported by the National Natural Science Foundation of China (Grant No. 41872045). We thank Dr. H. Yang at the University of Arizona for providing us with studied samples from the RRUFF Project.

References

Aguilar-Santillan J, Cuenca-Alvarez R, Balmori-Ramirez H, Bradt RC (2002) Mechanical activation of the decomposition and sintering of kyanite. J Am Ceram Soc 85:2425–2431

Bell PM (1963) Aluminum silicate system: experimental determination of the triple point. Science 139:1055–1056

Birch F (1961) The velocity of compressional waves in rocks to 10 kilobars: 2. J Geophys Res 66:2199–2224

Bohlen SR, Montana A, Kerrick DM (1991) Precise determinations of the equilibria kyanite-sillimanite and kyanite-andalusite and a revised triple point for Al_2SiO_5 polymorphs. Am Mineral 76:677–680

Brace WF, Scholz CH, La Mori PN (1969) Isothermal compressibility of kyanite, andalusite, and sillimanite from synthetic aggregates. J Geophys Res 74:2089–2098

Bradt RC (2008) The sillimanite minerals: andalusite, kyanite, and sillimanite. In: Shackelford JF, Doremus RH (eds) Ceramic and glass materials. Springer, Boston, pp 41–48

Burnham CW (1963a) Refinement of the crystal structure of sillimanite. Z Kristallogr 118:127–148

Burnham CW (1963b) Refinement of the crystal structure of kyanite. Z Kristallogr 118:337–360

Burnham CW, Buerger MJ (1961) Refinement of the crystal structure of kyanite. Z Kristallogr 115:269–290

Burt JB, Ross NL, Angel RJ, Koch M (2006) Equations of state and structures of andalusite to 9.8 GPa and sillimanite to 8.5 GPa. Am Mineral 91:319–326

Comodi P, Zanazzi PF, Poli S, Schmidt MW (1997) High-pressure behavior of kyanite: Compressibility and structural deformations. Am Mineral 82:452–459

Fei Y (1995) Thermal expansion. In: Ahrens TJ (ed) Mineral physics and crystallography: a handbook of physical constants, vol 2. American Geophysical Union, Washington, pp 29–44

Fortes AD (2019) Thermal expansion of the Al_2SiO_5 polymorphs, kyanite, andalusite and sillimanite, between 10 and 1573 K determined using time-of-flight neutron powder diffraction. Phys Chem Miner 46:687–704

Friedrich A, Kunz M, Winkler B, Le Bihan T (2004) High-pressure behavior of sillimanite and kyanite: compressibility, decomposition and indications of a new high-pressure phase. Z Kristallogr 219:324–329

Gatta GD, Nestola F, Walter JM (2006) On the thermo-elastic behaviour of kyanite: a neutron powder diffraction study up to 1200 ℃. Mineral Mag 70:309–317

Gillet P, Guyot F, Malezieux JM (1989) High-pressure, high-temperature Raman spectroscopy of Ca_2GeO_4 (olivine form): some insights on anharmonicity. Phys Earth Planet Inter 58:141–154

Gillet P, Fiquet G, Malezieux JM, Geiger CA (1992) High-pressure and high-temperature Raman spectroscopy of end-member garnets: pyrope, grossular and andradite. Eur J Mineral 4:651–664

Hemingway BS, Robie RA, Evans HT, Kenick DM (1991) Heat capacities and entropies of sillimanite, fibrolite, andalusite, kyanite, and quartz and the Al_2SiO_5 phase diagram. Am Mineral 76:1597–1613

Hofmeister AM, Chopelas A (1991) Thermodynamic properties of pyrope and grossular from vibrational spectroscopy. Am Miner 76:880–891

Holdaway MJ (1971) Stability of andalusite and the alumino-silicate phase diagram. Am J Sci 271:97–131

Hu X, Liu X, He Q, Wang H, Qin S, Ren L, Chang L (2011) Thermal expansion of andalusite and sillimanite at ambient pressure: a powder X-ray diffraction study up to 1000 ℃. Mineral Mag 75:363–374

Iishi K, Salje E, Werneke C (1979) Phonon spectra and rigid-ion model calculations on andalusite. Phys Chem Miner 4:173–188

Irifune T, Kuroda K, Minagawa T, Unemoto M (1995) Experimental study of the decomposition of kyanite at high pressure and high temperature. In: Yukutake T (ed) The Earth's central part: its structure and dynamics, Tokyo, pp 35–44

Kerrick DM (1990) The Al2SiO5 polymorphs. Reviews in mineralogy, vol 22. Mineralogical Society of American, Chantilly

Kieffer SW (1979a) Thermodynamics and lattice vibrations of minerals: 1. Mineral heat capacities and their relationships to simple lattice vibrational models. Rev Geophys 17:1–19

Kieffer SW (1979b) Thermodynamics and lattice vibrations of minerals: 3. Lattice dynamics and an approximation for minerals with application to simple substances and framework silicates. Rev Geophys 17:35–59

Kieffer SW (1980) Thermodynamics and lattice vibrations of minerals: 4. Application to chain and sheet silicate and orthosilicates. Rev Geophys 18:862–886

Kojitani H, Nishimura K, Kubo A, Sakashita M, Aoki K, Akaogi M (2003) Raman spectroscopy and heat capacity measurement of calcium ferrite type $MgAl_2O_4$ and $CaAl_2O_4$. Phys Chem Miner 30:409–415

Lazarev AN (1972) Vibrational spectra and structure of silicates. Consultants Bureau, New York-London

Liu LG (1974) Disproportionation of kyanite to corundum plus stishovite at high pressure and temperature. Earth Planet Sci Lett 24:224–228

Liu X, Nishiyama N, Sanehira T, Inoue T, Higo Y, Sakamoto S (2006) Decomposition of kyanite and solubility of Al_2O_3 in stishovite at high pressure and high temperature conditions. Phys Chem Miner 33:711–721

Liu X, Shieh SR, Fleet ME, Zhang L (2009) Compressibility of a natural kyanite to 17.5 GPa. Prog Nat Sci Mater 19:1281–1286

Liu X, He Q, Wang H, Fleet ME, Hu X (2010) Thermal expansion of kyanite at ambient pressure: an X-ray powder diffraction study up to 1000 ℃. Geosci Front 1:91–97

Lv MD (2016) Crystal structure and spectroscopy of aluminosilicate isomorphism. Dissertation, Peking University

Mammone JF, Sharma S (1979) Pressure and temperature dependence of the Raman spectra of rutile-structure oxides. Carnegie Institution Year Book, Washington, pp 369–373

Matsui M (1996) Molecular dynamics study of the structures and moduli of crystals in the system CaO-MgO-Al_2O_3–SiO_2. Phys Chem Miner 23:345–353

McMillan P, Piriou B (1982) The structures and vibrational spectra of crystals and glasses in the silica-alumina system. J Non Cryst Solids 53:279–298

Mernagh TP, Liu LG (1991) Raman spectra from the Al_2SiO_5 polymorphs at high pressures and room temperature. Phys Chem Miner 18:126–130

Momma K, Izumi F (2011) VESTA 3 for three-dimensional visualization of crystal, volumetric and morphology data. J Appl Crystallogr 44:1272–1276

Nakamoto K (2009) Infrared and raman spectra of inorganic and coordination compounds. Part B: applications in coordination, organometallic, and bioinorganic chemistry, 6th Edition, Wiley

Náray-Szabo S, Taylor WH, Jackson WW (1929) The structure of kyanite. Z Kristallogr 71:117–130

Oganov AR, Brodholt JP (2000) High-pressure phases in the Al_2SiO_5 system and the problem of aluminous phase in the Earth's lower mantle: ab initio calculations. Phys Chem Miner 27:430–439

Okada T, Narita T, Nagai T, Yamanaka T (2008) Comparative Raman spectroscopic study on ilmenite-type $MgSiO_3$ (akimotoite), $MgGeO_3$, and $MgTiO_3$ (geikielite) at high temperatures and high pressures. Am Mineral 93:39–47

Ono S, Nakajima Y, Funakoshi K (2007) In situ observation of the decomposition of kyanite at high pressures and high temperatures. Am Mineral 92:1624–1629

Pan F, Yu XH, Mo XX, You JL, Wang C, Chen H, Jiang GC (2006) Raman active vibrations of aluminosilicates. Spectrosc Spect Anal 26:1871–1875

Pankratz LB, Kelley KK (1964) High temperature heat contents and entropies of andalusite, kyanite and sillimanite. US Bur Mines Rep Invest 1964:6370

Ralph RL, Finger LW, Hazen RM, Ghose S (1984) Compressibility and crystal structure of andalusite at high pressure. Am Mineral 69:513–519

Rao MN, Chaplot SL, Choudhury N, Rao KR, Azuah RT, Montfrooij WT, Bennington SM (1999) Lattice dynamics and inelastic neutron scattering from sillimanite and kyanite Al_2SiO_5. Phys Rev B 60:12061–12068

Reynard B, Price GD, Gillet P (1992) Thermodynamic and anharmonic properties of forsterite, α-Mg_2SiO_4: computer modelling versus high-pressure and high-temperature measurements. J Geophys Res 97:19791–19801

Richardson SW, Gilbert MC, Bell PM (1969) Experimental determination of kyanite-andalusite and andalusite-sillimanite equilibria; the aluminum silicate triple point. Am J Sci 267:259–272

Robie RA, Hemingway BS (1984) Entropies of kyanite, andalusite, and sillimanite: additional constraints on the pressure and temperature of the Al_2SiO_5 triple point. Am Mineral 69:298–306

Salje E (1986) Heat capacities and entropies of andalusite and sillimanite: the influence of fibrolitization on the phase diagram of the Al_2SiO_5 polymorphs. Am Mineral 71:1366–1371

Salje E, Werneke C (1982) The phase equilibrium between sillimanite and andalusite as determined from lattice vibrations. Contrib Mineral Petrol 79:56–67

Schmidt MW, Poli S, Comodi P, Zanazzi PF (1997) High-pressure behavior of kyanite: decomposition of kyanite into stishovite and corundum. Am Mineral 82:460–466

Schneider H, Majdic A (1979) Kinetics and mechanism of the solid state high temperature transformation of andalusite (Al_2SiO_5) into 3/2 mullite, $3Al_2O_3{\cdot}2SiO_2$, and silica, SiO_2. Ceramurgia Int 5:31–36

Schneider H, Majdic A (1980) Kinetics of the thermal decomposition of kyanite. Ceram Int 6:32–37

Schneider H, Majdic A (1981) Preliminary investigation on the kinetics of the high-temperature transformation of sillimanite to 3/2 mullite, $3Al_2O_3{\cdot}2SiO_2$, and silica, SiO_2, and comparison with the behavior of andalusite and kyanite. Sci Ceram 11:191–196

Skinner BJ, Clark SP, Appleman DE (1961) Molar volumes and thermal expansions of andalusite, kyanite, and sillimanite. Am J Sci 259:651–668

Taylor WH (1928) The structure of sillimanite and mullite. Z Kristallogra 68:503–521

Taylor WH (1929) The structure of andalusite, Al_2SiO_5. Z Kristallogr 71:205–218

Todd SS (1950) Heat capacities at low temperatures and entropies at 298.16° K of andalusite, kyanite, and sillimanite. J Am Chem Soc 72:4742–4743

Vaughan MT, Weidner DJ (1978) The relationship of elasticity and crystal structure in andalusite and sillimanite. Phys Chem Miner 3:133–144

Winkler B, Hytha M, Warren MC, MilmanV GJD, Schreuer J (2001) Calculation of the elastic constants of the Al_2SiO_5 polymorphs andalusite, sillimanite and kyanite. Z Kristallogr 216:67–70

Winter JK, Ghose S (1979) Thermal expansion and high-temperature crystal chemistry of the Al_2SiO_5 polymorphs. Am Mineral 64:573–586

Wu C, Zhao G (2007) The metapelitic garnet-biotite-muscovite-aluminosilicate- quartz (GBMAQ) geobarometer. Lithos 97:365–372

Xue W, Zhai K, Lin CC, Zhai S (2018) Effect of temperature on the Raman spectra of $Ca_5(PO_4)_3F$ fluorapatite. Eur J Mineral 30:951–956

Yang H, Downs RT, Finger LW, Hazen RM, Prewitt CT (1997a) Compressibility and crystal structure of kyanite, Al_2SiO_5, at high pressure. Am Mineral 82:467–474

Yang H, Hazen RM, Finger LW, Prewitt CT, Downs RT (1997b) Compressibility and crystal structure of sillimanite, Al_2SiO_5, at high pressure. Phys Chem Miner 25:39–47

Zhou Y, Irifune T, Ohfuji H, Kuribayashi T (2018) New high-pressure forms of Al_2SiO_5. Geophys Res Lett 45:8167–8172